# Chiral Lagrangian parameters for scalar and pseudoscalar mesons

W. Bardeen and E. Eichten
*Fermilab, P. O. Box 500, Batavia, Illinois 60510, USA*

H. Thacker
*Department of Physics, University of Virginia, Charlottesville, Virginia 22901, USA*

(Received 22 July 2003; published 24 March 2004)

The results of a high-statistics study of scalar and pseudoscalar meson propagators in quenched lattice QCD are presented. For two values of lattice spacing, $\beta=5.7$ ($a\approx.18$ fm) and 5.9 ($a\approx.12$ fm), we probe the light quark mass region using clover improved Wilson fermions with the modified quenched approximation pole-shifting ansatz to treat the exceptional configuration problem. The quenched chiral loop parameters $m_0$ and $\alpha_\Phi$ are determined from a study of the pseudoscalar hairpin correlator. From a global fit to the meson correlators, estimates are obtained for the relevant chiral Lagrangian parameters, including the Leutwyler parameters $L_5$ and $L_8$. Using the parameters obtained from the singlet and nonsinglet pseudoscalar correlators, the quenched chiral loop (QCL) effect in the nonsinglet scalar meson correlator is studied. By removing this QCL effect from the lattice correlator, we obtain the mass and decay constant of the ground state scalar, isovector meson $a_0$.

DOI: 10.1103/PhysRevD.69.054502 PACS number(s): 12.38.Gc, 11.15.Ha, 11.30.Rd, 12.39.Fe

## I. INTRODUCTION

Improved methods for studying the regime of small quark mass in lattice QCD provide the realistic prospect of quantitatively determining the parameters of the low energy chiral Lagrangian of QCD from first principles. Although a definitive comparison with experiment requires the analysis of full and/or partially quenched simulations, detailed studies of chiral behavior in the quenched approximation are of interest for several reasons. First, the characteristic quenched chiral loop effects which arise from the anomalous double-pole structure of the quenched, flavor-singlet pseudoscalar propagator will also occur in partially quenched calculations (at a level determined by the mismatch between valence and sea quark masses) [1]. The observation of these anomalous effects in the quenched theory should provide a useful baseline for future chiral analysis of full QCD. Second, although it is not a unitary theory, the quenched approximation can be analyzed in an effective Lagrangian framework [2,3], yielding a well-defined set of low-energy constants in quenched chiral perturbation theory. [In practice, this requires the assumption that the $U_A(1)$ breaking from the anomaly can also be treated perturbatively.] A comparison of these constants with those of full QCD can provide valuable insight into the role of closed quark loops in hadron phenomenology. In addition, the study of chiral behavior in the quenched approximation provides useful information about the interplay between topological charge and chiral symmetry breaking in QCD. For example, the Witten-Veneziano formula relates the gluonic component of the $\eta'$ mass in full QCD to the topological susceptibility of the quenched theory.

In two previous papers [4,5] we reported results of a study of the chiral behavior of scalar and pseudoscalar meson propagators in quenched QCD at $\beta=5.7$ using clover improved Wilson fermions. In this paper we present results from a new data set at $\beta=5.9$ [6], compare them with the $\beta=5.7$ results, and summarize the main conclusions of this study. We also compare our results to those of other recent studies [7]. An important ingredient in our analysis is the use of the modified quenched approximation (MQA) pole-shifting procedure [9] to resolve the exceptional configuration problem. Our experience with this technique has led us to conclude that it provides a practical and quantitatively acceptable resolution of the problem, which eliminates the spurious statistical fluctuations of exceptional configurations without systematically biasing the final results. This conclusion is based on the consistency between the light-quark results and those of heavier quarks where the pole shifting has a negligible effect on the propagators. It is also supported by the overall agreement we observe between our results (in and out of the pole region) and theoretical expectations based on quenched chiral perturbation theory (see Sec. VI).

Since the introduction of the MQA procedure, other methods for avoiding the exceptional configuration problem have been explored. These include twisted-mass QCD [10] and the use of exactly chiral (overlap [11] or domain-wall [12]) fermions. All these approaches have in common the fact that Wilson-Dirac eigenvalues at positive real quark mass are eliminated, thus resolving the problem. It should be noted that exactly real eigenmodes of the Wilson-Dirac operator, which are the cause of the exceptional configuration problem, make a negligible contribution to physical quantities in the infinite volume limit (vanishing like $1/\sqrt{V}$). Thus any prescription which effectively removes these poles from the physical region should provide a satisfactory resolution of the problem for sufficiently large volume. The MQA pole shifting is a minimal prescription for accomplishing this. A more stringent test of the procedure is the study of chiral behavior for very light quarks in a *finite* volume which is large compared to the QCD scale but comparable to the chiral scale. In this regime, finite volume effects are large but calculable in quenched chiral perturbation theory (Q$\chi$PT), simply by replacing loop integrals by finite-volume momentum sums. As discussed in [5], the scalar, isovector (valence) meson propagator exhibits a prominent quenched chiral loop effect arising from the $\eta'$-$\pi$ intermediate state. For the light-

 

est quark masses we study, the finite volume effects expected from Q$\chi$PT are quite large. Thus, the detailed agreement (as a function of both time and pion mass) between the measured scalar propagator and the *finite-volume* one-loop calculation provides a convincing demonstration that the MQA procedure is an effective method for exploring the light quark regime with Wilson fermions.

## II. QUENCHED CHIRAL PERTURBATION THEORY

To analyze the quenched theory in a chiral Lagrangian framework, one introduces wrong-statistics ghost quark fields to cancel closed loops, yielding a low-energy chiral Lagrangian with a graded $U(3|3)\times U(3|3)$ symmetry [2]. At the one-loop level, this is equivalent to the simpler and more direct approach to quenched $\chi$PT [3] which begins with an ordinary $U(3)\times U(3)$ chiral Lagrangian describing a nonet of Goldstone bosons. To leading order, this is

$$\mathcal{L}_2=\frac{f^2}{4}[\mathrm{tr}(\partial_\mu U^\dagger \partial^\mu U)+\mathrm{tr}(\chi^\dagger U+U^\dagger \chi)] \tag{1}$$

where $U$ is a $U(3)\times U(3)$ chiral field and $\chi$ is the pseudoscalar mass matrix. Our analysis also incorporates the following fourth-order terms in the chiral Lagrangian [14]:

$$\mathcal{L}_4=L_5\mathrm{tr}[\partial_\mu U^\dagger \partial^\mu U(\chi^\dagger U+U^\dagger \chi)] + L_8\mathrm{tr}(\chi^\dagger U\chi^\dagger U+U^\dagger \chi U^\dagger \chi). \tag{2}$$

The effect of the axial $U(1)$ anomaly is introduced as an explicit symmetry breaking term consisting of a flavor-singlet pseudoscalar $\eta'$ mass term and a field renormalization,

$$\mathcal{L}_{hp}=\frac{1}{2}(\alpha_\Phi \partial^\mu \eta' \partial_\mu \eta' - m_0^2 \eta'^2) \tag{3}$$

where

$$\eta'=\frac{f}{2}(i\,\mathrm{tr}\ln(U^\dagger)-i\,\mathrm{tr}\ln(U)). \tag{4}$$

Finally, we will also analyze the scalar, isovector meson propagator, which turns out to be well described by a combination of a heavy $a_0$ meson and an $\eta'$-$\pi$ loop diagram. Thus, we incorporate a scalar-isovector meson field, using the formalism of nonlinear chiral Lagrangians [4],

$$\mathcal{L}_{sc}=\frac{1}{4}\mathrm{tr}\{D\sigma D\sigma\}-\frac{1}{4}m_s^2\mathrm{tr}\{\sigma\sigma\} + f_s\mathrm{tr}\{\chi^\dagger\sqrt{U}\sigma\sqrt{U}+\chi\sqrt{U^\dagger}\sigma\sqrt{U^\dagger}\} \tag{5}$$

where $D$ is a chirally covariant derivative. One of our motivations for studying the scalar correlator is the expectation of a prominent quenched chiral loop effect from the $\eta'$-$\pi$ intermediate state, as discussed in Ref. [5]. The agreement between the lattice correlator and the one-loop calculation is very good, particularly for the $\beta=5.9$ results, as discussed in Sec. VI.

To summarize, the low energy chiral Lagrangian used in our analysis is

$$\mathcal{L}=\mathcal{L}_2+\mathcal{L}_4+\mathcal{L}_{hp}+\mathcal{L}_{sc}. \tag{6}$$

In the quenched approximation, we have the supplementary rule that multiple $\eta'$ mass insertions on a given pseudoscalar line are excluded. More generally, any $\chi$PT diagram corresponding to a quark-line diagram with internal closed loops is discarded [3]. At the one-chiral-loop level, these rules are unambiguous, and equivalent to the more systematic procedure of introducing ghost fields [2].

## III. LATTICE PARAMETERS

The calculations discussed in this paper were carried out on the Fermilab ACPMAPS and on the UVA Linux cluster GARCIA. The two Monte Carlo gauge ensembles analyzed consisted of 300 configurations at $\beta=5.7$ on a $12^3\times 24$ lattice, and 350 configurations at $\beta=5.9$ on a $16^3\times 32$ lattice (the Fermilab *b* and *c* ensembles). Quark propagators were calculated with clover improved Wilson action. The clover coefficients used were $C_{sw}=1.57$ for $\beta=5.7$ and $C_{sw}=1.50$ for $\beta=5.9$. For $\beta=5.7$, the quark propagators were calculated for $\kappa=.1410,.1415,.1420,.1423,.1425,.1427$, and .1428, with $\kappa_c=.14329$, while for $\beta=5.9$, propagators were calculated with $\kappa=.1382,.1385,.1388,.1391,.1394$, and .1397, with $\kappa_c=.14013$. In physical units, this corresponds to a range of pion masses of 275 to 565 MeV for $\beta=5.7$ and 330 to 665 MeV for $\beta=5.9$. Here and elsewhere, we will quote results in physical units using the rho mass to set the scale.

An analysis of smeared and local rho propagators on our ensembles yields $m_\rho a=.690(8)$ and .469(3) for $\beta=5.7$ and $\beta=5.9$, respectively. An analysis of the axial-vector meson channel also yields a mass for the $a_1$ meson of 1.15(7) and 0.77(3) for $\beta=5.7$ and $\beta=5.9$ respectively. Using the rho mass to fix the scale gives $a^{-1}=1.12$ GeV for $\beta=5.7$ and 1.64 GeV for $\beta=5.9$. The resulting physical mass for the $a_1$ (1290 MeV for $\beta=5.7$ and 1260 MeV for $\beta=5.9$) is close to the mass of the observed $a_1(1260)$ resonance.

To get some idea of the systematic error associated with choice of scale, we will sometimes quote equivalent results using the charmonium $1S$-$1P$ splitting scales of 1.18 GeV and 1.80 GeV for the two ensembles. The MQA pole-shifting procedure [9] was applied to all quark propagators. For $\beta=5.7$, all poles below $\kappa=.1431$ were located and shifted, while for $\beta=5.9$, all poles below $\kappa=.1400$ were shifted.

## IV. THE HAIRPIN INSERTION, $\eta'$ MASS, AND TOPOLOGICAL SUSCEPTIBILITY

We begin by determining the parameters $m_0$ and $\alpha_\Phi$ in the term $\mathcal{L}_{hp}$, Eq. (3). These parameters are extracted from the two-quark-loop ("disconnected") piece of the quenched flavor singlet pseudoscalar correlator,

$$\Delta_h(x)=\langle \mathrm{tr}\,\gamma^5 G(x,x)\mathrm{tr}\,\gamma^5 G(0,0)\rangle. \tag{7}$$

The lowest order Q$\chi$PT approximation to Eq. (7) is the tree graph with a single hairpin insertion between two pion propagators. In momentum space, this is

$$\tilde{\Delta}_h(p) = f_P \frac{1}{p^2+m_\pi^2}(m_0^2+\alpha_\Phi p^2)\frac{1}{p^2+m_\pi^2} f_P \tag{8}$$

where $f_P$ is the pseudoscalar decay constant,

$$f_P = \langle 0|\bar{\psi}\gamma^5\psi|\pi\rangle. \tag{9}$$

Fourier transforming over $p_0$ and setting $\vec{p}=0$, we have

$$\Delta_h(\vec{p}=0,t) = \frac{f_P^2}{4m_\pi^3}[C_+ + C_- m_\pi t]e^{-m_\pi t} + (t \to T-t) \tag{10}$$

where

$$C_\pm \equiv m_0^2 \pm \alpha_\Phi m_\pi^2. \tag{11}$$

In our previous analysis of the $\beta=5.7$ ensemble, the hairpin correlator $\Delta_h$ was studied for both local and smeared sources and compared with the pion pole residues of the corresponding valence propagators. This analysis demonstrated a remarkable absence of excited state contamination in the hairpin correlator, even when the sources were separated by only one or two time slices. Moreover, the time dependence of $\Delta_h(t)$ was well described at all times $t \geqslant 2$ by the formula (10) with $\alpha_\Phi=0$, i.e. by a pure momentum-independent mass insertion. For the present analysis, we have fitted both the 5.7 and 5.9 ensembles to the full two-parameter formula (10) in order to obtain an accurate estimate of $\alpha_\Phi$. For the 5.7 ensemble, acceptable $\chi^2$'s were obtained by fitting a range of times from $t=3$ to 12. Using the fully correlated error matrix, the covariant $\chi^2$ for these fits ranged from 0.8 to 1.5 per degree of freedom. For the hairpin correlators at $\beta=5.9$, we obtained very good fits to the formula (10) over the entire time range from $t=1$ to 16. Here the correlated $\chi^2$'s ranged from 0.3 to 0.5 per degree of freedom. An example of a hairpin fit for $\beta=5.9$ and $\kappa=.1394$ is shown in Fig. 1. The solid line is the pure dipole fit with $\alpha_\Phi=0$. In Tables I and II we give the $\beta=5.7$ and 5.9 results for $m_0$ and $\alpha_\Phi$. Also shown in the last column are the values of $m_0$ obtained from the 1-parameter pure dipole fit with $\alpha_\Phi=0$. Considering first the results for $\alpha_\Phi$, the values for the 5.7 ensemble are negative by about one to two standard deviations, while the values for $\beta=5.9$ are slightly positive, also by about two standard deviations. The values for different $\kappa$'s within each ensemble are highly correlated, so the deviation of $\alpha_\Phi$ from zero in either data set has little statistical significance. Ignoring $\kappa$ dependence and averaging the values within each ensemble, we get

$$\alpha_\Phi = -0.15 \pm 0.10, \quad \beta=5.7 \tag{12}$$

and

$$\alpha_\Phi = 0.05 \pm 0.03, \quad \beta=5.9. \tag{13}$$

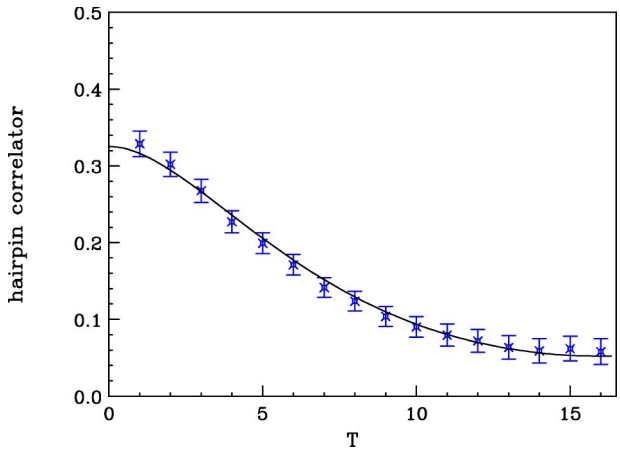


FIG. 1. The quenched hairpin correlator for $\beta=5.9$, $\kappa=.1394$. The solid line is a pure dipole fit with $\alpha_\Phi=0$.

If we ignore any possible lattice spacing dependence and average the two data sets in quadrature, we get the final result

$$\alpha_\Phi = 0.03 \pm 0.03. \tag{14}$$

This can be regarded as a success of the large-$N_c$ view of the anomaly where this renormalization is an order $1/N_c$ effect. In the subsequent analysis we will take $\alpha_\Phi=0$.

Fitting the hairpin correlators to the pure dipole $\alpha_\Phi=0$ form (last column of Tables I and II) we obtain the chirally extrapolated values (in lattice units)

$$m_0 = .348(4), \quad \beta=5.7 \tag{15}$$

and

$$m_0 = .232(4), \quad \beta=5.9. \tag{16}$$

Using the rho mass scale and including a flavor factor of $\sqrt{3}$, this gives the gluonic component of the $\eta'$ mass

$$m_{\eta'}^{glue} = 675(8) \text{ MeV}, \quad \beta=5.7 \tag{17}$$

$$= 659(12) \text{ MeV}, \quad \beta=5.9. \tag{18}$$

If we instead use the charmonium scale we get

$$m_{\eta'}^{glue} = 712(9) \text{ MeV}, \quad \beta=5.7 \tag{19}$$

$$= 723(13) \text{ MeV}, \quad \beta=5.9. \tag{20}$$

We conclude that the $\eta'$ mass scales reasonably well between $\beta=5.7$ and 5.9, well within the systematic uncertainty associated with different ways of determining the lattice spacing. The values we obtain for the $\eta'$ mass insertion are somewhat low compared to the estimate of $\approx 850$ MeV obtained from the physical $\eta'$ mass and chiral perturbation theory. Although we see approximate scaling, it would require calculations at larger values of $\beta$ to rule out a significant lattice spacing effect. It is also worth remembering that the whole framework in which the quenched hairpin diagram is interpreted as a mass insertion is demonstrably valid only

TABLE I. Fit parameters $m_0$ and $\alpha_\Phi$ for the $\beta=5.7$ hairpin correlators. All masses are in lattice units.

| $\kappa$ | $m_\pi$ | $m_0$ | $\alpha_\Phi$ | $m_0(\alpha_\Phi=0)$ |
|---|---|---|---|---|
| .1410 | .505(2) | .269(26) | −.17(10) | .280(10) |
| .1415 | .450(3) | .291(24) | −.18(10) | .294(10) |
| .1420 | .386(3) | .310(21) | −.19(10) | .308(10) |
| .1423 | .342(4) | .321(19) | −.19(10) | .316(10) |
| .1425 | .307(4) | .326(19) | −.16(11) | .321(10) |
| .1427 | .267(5) | .326(19) | −.10(12) | .322(11) |
| .1428 | .245(6) | .323(19) | −.03(13) | .322(11) |

in the limit of large $N_c$, so some discrepancy between the lattice calculation of $m_0$ and the phenomenological estimate might be expected. A recent calculation of the $\eta'$ mass in two-flavor *full* QCD by the CPPACS Collaboration [13] gave the result $m_{\eta'}=960(87)^{+36}_{-286}$ MeV, in good agreement with experiment. Detailed comparisons between quenched and full QCD studies of the $\eta'$ should provide a better understanding of the accuracy of large-$N_c$ arguments in the framework of chiral Lagrangians.

The overall size of quenched chiral loop (QCL) effects is determined by the parameter $\delta$, which can be computed from the hairpin insertion mass $m_0$ and the axial vector decay constant $f_A$ (evaluated in the next section),

$$\delta=\frac{m_0^2}{24\pi^2 f_A^2}. \tag{21}$$

Using the chirally extrapolated values of $m_0$ and $f_A$, we obtain

$$\delta=.099(3), \quad \beta=5.7 \tag{22}$$

and

$$\delta=.108(4), \quad \beta=5.9. \tag{23}$$

It is interesting to consider not only the value of $\delta$ in the chiral limit, but also the effective value of $\delta$ at a given quark mass by computing the quantity (21) from the values of $m_0$ and $f_A$ at that mass. The values of $\delta_{eff}$ vs $m_\pi^2$ for both $\beta=5.7$ and 5.9 are plotted in Fig. 2. This plot shows a rather strong quark mass dependence of the effective QCL parameter, which may provide at least a partial explanation of the

TABLE II. Fit parameters $m_0$ and $\alpha_\Phi$ for the $\beta=5.9$ hairpin correlators. All masses are in lattice units.

| $\kappa$ | $m_\pi$ | $m_0$ | $\alpha_\Phi$ | $m_0(\alpha_\Phi=0)$ |
|---|---|---|---|---|
| .1382 | .411(3) | .188(14) | .04(2) | .194(5) |
| .1385 | .378(3) | .192(13) | .04(2) | .198(5) |
| .1388 | .343(4) | .197(11) | .04(2) | .203(5) |
| .1391 | .304(4) | .204(11) | .05(2) | .209(5) |
| .1394 | .261(5) | .211(9) | .06(3) | .217(5) |
| .1397 | .204(5) | .220(9) | .11(4) | .226(6) |

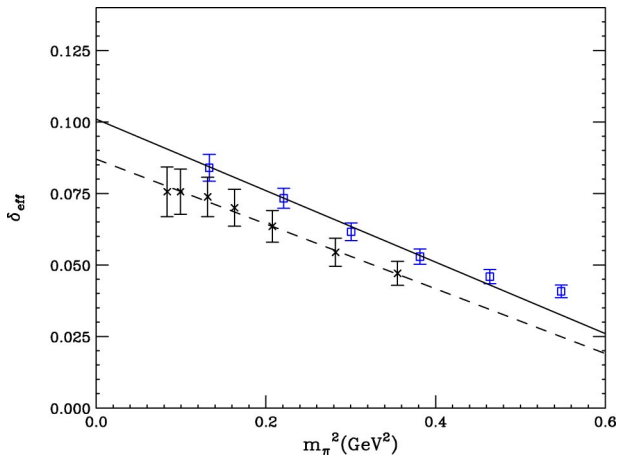


FIG. 2. The quenched chiral log parameter $\delta_{eff}$ vs squared pion mass, $m_\pi^2$. Results from both $\beta=5.7$ ($\times$'s) and 5.9 (boxes) are plotted. The linear fits include all mass values for $\beta=5.7$ and the four lightest masses for $\beta=5.9$.

fact that many of the determinations of $\delta$ from lattice studies of quenched chiral logs [7] have favored a value of $\delta$ substantially smaller than the phenomenological estimate of $\delta\approx 0.17$. From Fig. 2 we see that, for pion masses $>300$ MeV where most studies have been carried out, the value of $\delta_{eff}$ is smaller than the value in the chiral limit by as much as a factor of two. The decrease of $\delta_{eff}$ with increasing quark mass represents the combined effect of a decreasing value of $m_0$ and an increasing value of $f_A$ as the quark mass increases. Although the negative slope of $\delta_{eff}$ has the effect of suppressing quenched chiral logs, it is nevertheless more consistent to treat $\delta$ as a constant in fitting to chiral Lagrangian parameters, since the effective mass dependence should arise from higher order terms in the chiral expansion. This is the procedure we adopt in the subsequent analysis of the scalar and pseudoscalar correlators, where the best Q$\chi$PT fit favors a value of $\delta$ about half as large as that obtained from the chirally extrapolated hairpin result. We might expect to find a larger value of $\delta$ if studies were carried out well below $m_\pi=300$ MeV. [It is interesting that a recent study [15] using overlap fermions, which went as low as $m_\pi=180$ MeV, found a large value of $\delta$. However, the value $\delta=0.26(3)$ obtained in Ref. [15] is much larger than even our chirally extrapolated result of 0.108(4), indicating that there are other systematic differences in the calculations. Further chiral studies comparing different fermion actions on the same gauge configurations would be of considerable interest.]

The ''allsource'' quark propagators used to calculate the hairpin correlators [16] can also be used to calculate the topological susceptibility. Using the integrated anomaly method [17,4], we calculate a winding number for each gauge configuration from the pseudoscalar charge integrated over the whole lattice. From these winding numbers, we compute the topological susceptibility $\chi_t=\langle\nu^2\rangle/V$. Using the rho scale, this gives

$$\chi_t=(178(4)\ \text{MeV})^4, \quad \beta=5.7 \tag{24}$$

$$= (171(3)\ \ \mathrm{MeV})^4, \quad \beta = 5.9. \tag{25}$$

Results quoted previously [4] used the charmonium scale, which gives

$$\chi_t = (188(4)\ \ \mathrm{MeV})^4, \quad \beta = 5.7 \tag{26}$$

$$= (188(3)\ \ \mathrm{MeV})^4, \quad \beta = 5.9. \tag{27}$$

## V. PSEUDOSCALAR MASSES AND DECAY CONSTANTS

The one-loop chiral Lagrangian analysis of the pseudoscalar and axial-vector propagators for the $\beta = 5.7$ ensemble has been described previously [4]. Here we briefly review that analysis and compare the previously reported results with the new results at $\beta = 5.9$. We also compare with results of the Alpha Collaboration [7,8] and discuss some issues associated with extracting the Leutwyler parameters $L_5$ and $L_8$, or correspondingly $\alpha_5$ and $\alpha_8$. [Note: Here and elsewhere, we use a conventional notation for the rescaled parameters: $\alpha_i = 8(4\pi)^2 L_i$.]

For both ensembles, we calculated propagators using smeared pseudoscalar, local pseudoscalar, and local axial-vector sources and sinks. The calculations were done for all meson propagators with both degenerate and nondegenerate quark masses. The chiral Lagrangian parameters were extracted from a global fit to all pseudoscalar masses and decay constants based on one-loop quenched $\chi$PT for the Lagrangian $\mathcal{L}_2 + \mathcal{L}_4 + \mathcal{L}_{hp}$, as discussed in Sec. III. For the lightest pion masses we studied, finite volume effects on chiral loop integrals are potentially significant, so all one-loop calculations were carried out with the appropriate finite-volume momentum sums rather than loop integrals. In addition, quadratic and logarithmically divergent integrals are regularized by subtraction at a cutoff scale $\Lambda \approx 1/a$. To summarize, a generic loop integral of the form

$$I_{ij} = \frac{1}{\pi^2} \int d^4p \frac{1}{p^2 + M_i^2} \frac{1}{p^2 + M_j^2} \tag{28}$$

is replaced by a cutoff momentum sum

$$I_{ij} = 16\pi^2 \sum_p \left( D(p_i, M_i) D(p_j, M_j) - D(p, \Lambda)^2 \right) \tag{29}$$

while a quadratically divergent integral

$$I_i = \frac{1}{\pi^2} \int \frac{d^4p}{p^2 + M_i^2} \tag{30}$$

is replaced by

$$I_i = 16\pi^2 \sum_p \left( D(p, M_i) - D(p, \Lambda) - (\Lambda^2 - M_i^2) D(p, \Lambda)^2 \right). \tag{31}$$

In these expressions, $D(p,M)$ is the free boson propagator and the momentum sums are defined according to the physical size of the corresponding lattice volume. With these definitions, the value of the squared pseudoscalar meson mass up to first order in $L_5$, $L_8$, and $\delta$ is

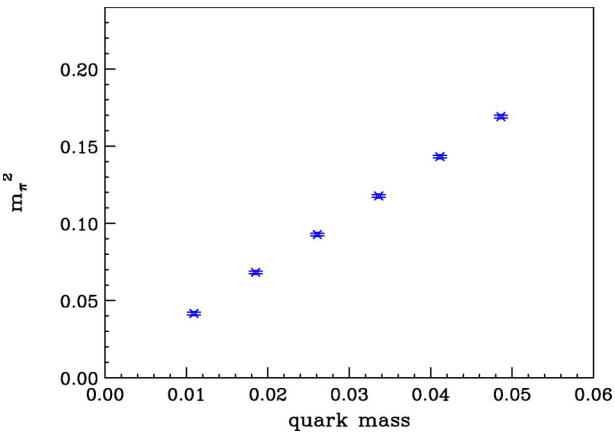


FIG. 3. Pion mass squared $m_\pi^2$ for equal quark masses for the $\beta = 5.9$ ensemble.

$$M_{ij}^2 = \chi_{ij}(1 + \delta I_{ij}) \left\{ 1 + \frac{1}{f^2} 8(2L_8 - L_5)\chi_{ij}[1 + \delta(\tilde{I}_{ij} + I_{ij})] + \frac{1}{f^2} 8L_5 \chi_{ij} \delta \tilde{J}_{ij} \right\} \tag{32}$$

where $r_0$ is a slope parameter, $\chi_i = 2r_0 m_i$, $\chi_{ij} = (\chi_i + \chi_j)/2$ and $m_i \equiv \ln[1 + 1/(2\kappa_i) - 1/(2\kappa_c)]$. Here $\tilde{I}_{ij} = (I_{ii}\chi_i + I_{jj}\chi_j)/\chi_{ij}$,

$$J_{ij} \equiv (I_i + I_j - (M_{ii}^2 + M_{jj}^2) I_{ij})/2, \tag{33}$$

$\tilde{J}_{ij} = J_{ij}/\chi_{ij}$. The fits for the pseudoscalar masses are shown in Figs. 3 and 4.

For the pseudoscalar decay constants:

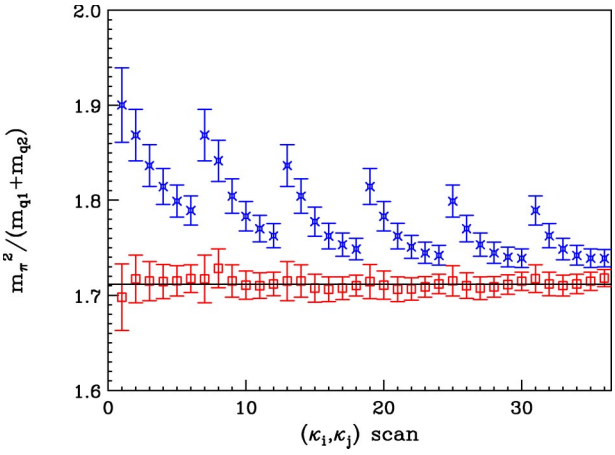


FIG. 4. Chiral slope parameter scan for $\beta = 5.9$. Individual chiral slopes are denoted by $(\times)$. The scan number is $6 \times (i-1) + j$ for the pair of $\kappa$ values $(\kappa_i, \kappa_j)$. The six $\kappa$ values are ordered from lightest to heaviest quark mass. Also shown are the ratios to the chiral log fit (boxes) which yields a global average of 1.712(39).

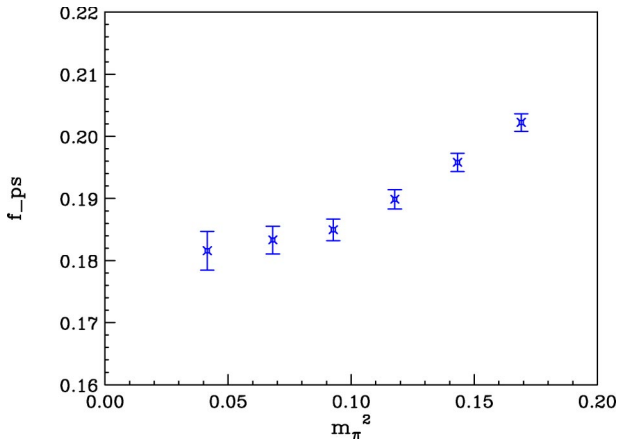


FIG. 5. Pseudoscalar decay constant, $f_{\rm ps}$, versus pion mass squared, $m_\pi^2$, for the $\beta=5.9$ ensemble. Only values for equal quark masses are shown. $f_{\rm ps}$ denotes the bare value of $f_{\rm P}$ in lattice units.

$$f_{P;ij}=\sqrt{2}fr_0[1+0.25\delta(I_{ii}+I_{jj}+2I_{ij})] \times\left\{1+\frac{4}{f^2}(4L_8-L_5)\chi_{ij}[1+\delta(\tilde{I}_{ij}+I_{ij})] -\frac{4}{f^2}L_5\delta\chi_{ij}\left[\left(\frac{\tilde{I}_{ij}}{2}+I_{ij}\right)-(\tilde{J}_{ii}+\tilde{J}_{jj})\right]\right\}. \quad (34)$$

The fits for the pseudoscalar decay constants are shown in Figs. 5 and 6.

For the axial vector decay constants, we have

$$f_{A;ij}=\sqrt{2}f[1+0.25\delta(I_{ii}+I_{jj}-2I_{ij})] \times\left\{1+\frac{4}{f^2}\chi_{ij}L_5[1+\delta(2I_{ij}-\tilde{I}_{ij})]\right\}. \quad (35)$$

The fits for the axial vector decay constants are shown in Figs. 7 and 8. In Figs. 4, 6, and 8 we show both the measured

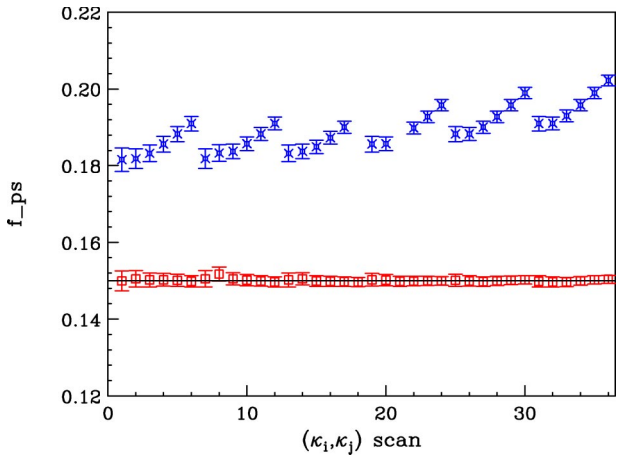


FIG. 6. Pseudoscalar decay constant scan for $\beta=5.9$. Also shown are the ratios to the chiral log fit which yields a global average $f_{\rm ps}=0.1501(77)$. The $(\kappa_i,\kappa_j)$ values are ordered as in Fig. 4.

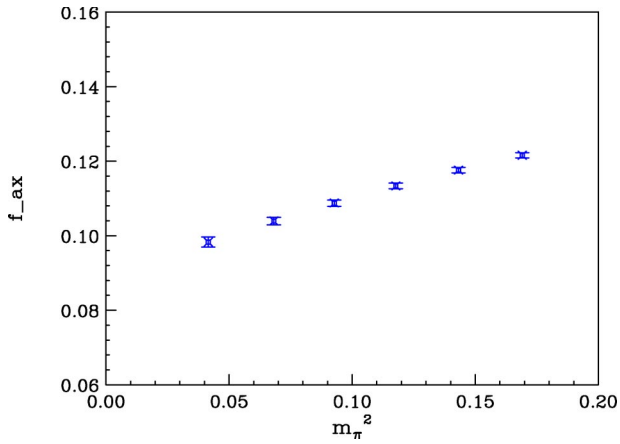


FIG. 7. Axial vector decay constant, $f_{\rm ax}$, versus pion mass squared, $m_\pi^2$, for the $\beta=5.9$ ensemble. Only values for equal quark masses are shown. $f_{\rm ax}$ denotes the bare value of $f_{\rm A}$ in lattice units.

values and the ratio values where the fitted chiral log factors in Eqs. (32), (34) and (35) have been divided out. The results are scanned over all combinations of the quark mass values.

The chiral Lagrangian parameters listed in Table III are the result of a global correlated fit of the Q$\chi$PT expressions to masses and decay constants with both equal and unequal quark masses. The results obtained from this global fit are generally consistent with evaluations extracted from more limited fits to equal quark mass data. In particular, the value $L_5$ may be estimated directly from the axial vector decay constant $f_A$. For equal quark masses $f_A$ has no quenched chiral logs, so the mass dependence should be linear in the chiral limit,

$$f_A=A+Bm_\pi^2. \quad (36)$$

[Note that in our notation, $f_A$ includes a factor of $\sqrt{(2)}$ relative to $f_\pi$, i.e. its physical value is 132 MeV.] A determination of $L_5$ is obtained from the product of slope and intercept:

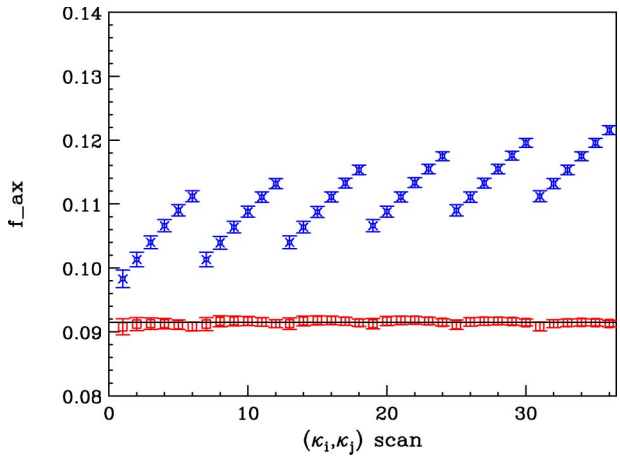


FIG. 8. Axial vector decay constant scan, $f_{\rm ax}$, for $\beta=5.9$. Also shown are the ratios to the chiral log fit which yields a global average $f_{\rm ax}=0.0915(13)$. The $(\kappa_i,\kappa_j)$ values are ordered as in Fig. 4.

TABLE III. Best fit for the chiral Lagrangian parameters for the $\beta=5.7$ and $\beta=5.9$ lattices.

| Parameter | $\beta=5.9$ | $\beta=5.7$ |
|---|---|---|
| $f=f_\pi$ | 0.091(2) | 0.100(2) |
| $L_5\times 10^3$ | 1.55(27) | 1.78(35) |
| $(L_8-L_5/2)\times 10^3$ | 0.02(5) | 0.14(7) |
| $r_0$ | 1.71(8) | 1.99(12) |
| $\delta$ | 0.053(13) | 0.059(15) |

$$L_5=\frac{A\cdot B}{8}. \tag{37}$$

Note that $A$ has units of mass and $B$ has units of $(\text{mass})^{-1}$, so that $L_5$ is dimensionless and can be evaluated without reference to a mass scale.

We obtain the results (in GeV using the rho scale)

$$f_A=[.1653(17)+.117(5)m_\pi^2]\times Z_A \ \text{GeV}, \quad \beta=5.7 \tag{38}$$

and

$$f_A=[.1515(20)+.106(7)m_\pi^2]\times Z_A \ \text{GeV}, \quad \beta=5.9. \tag{39}$$

Using $Z_A=0.845$ and 0.865 for $\beta=5.7$ and 5.9, respectively, we find

$$L_5(10^3)=1.72(11), \quad \alpha_5=2.18(14), \quad \beta=5.7 \tag{40}$$

and

$$L_5(10^3)=1.50(9), \quad \alpha_5=1.89(11), \quad \beta=5.9. \tag{41}$$

These values are consistent with the global fit results in Table III.

While this method is insensitive to the physical scale parameter the values of $L_5$ $(\alpha_5)$ are quite sensitive to the value of the axial vector renormalization constant, being proportional to $Z_A^2$. In the context of the tadpole renormalization scheme [18] our results in Eqs. (40), (41) include perturbative values for the renormalization constants as derived from the formulas given in Ref. [19].

As an alternative method, we could determine $L_5$ $(\alpha_5)$ from the ratio of the slope and intercept and the physical value of $f_\pi=93$ MeV. $L_5$ is now given by

$$L_5=f_\pi^2\frac{B}{4A}. \tag{42}$$

This result is independent of the renormalization factors $Z_A$ but will be sensitive to the choice of the physical scale parameter. This method is equivalent to choosing the renormalization factors so that the intercept correctly reproduces the physical value of $f_\pi$. Fixing the scale with the rho mass, the effective renormalization constants are $Z_A=0.80$ for $\beta=5.7$ and $Z_A=0.87$ for $\beta=5.9$. Using these effective renormalization constants modifies our predictions to

$$L_5(10^3)=1.54(10), \quad \alpha_5=1.95(13), \quad \beta=5.7 \tag{43}$$

$$L_5(10^3)=1.52(9), \quad \alpha_5=1.91(11), \quad \beta=5.9. \tag{44}$$

These values for $L_5$ $(\alpha_5)$ are consistent with our previous determinations using the product method.

The Alpha Collaboration [8] has recently made a careful analysis of quenched chiral Lagrangian parameters using an infrared insensitive ratio method. By using a series of lattices with $\beta$ values ranging from 6.0 to 6.45, they quote a continuum extrapolation for the value of $\alpha_5$,

$$\alpha_5=0.99(6). \tag{45}$$

This value is considerably smaller than the result we obtained on somewhat coarser lattices with $\beta$ values 5.7 and 5.9. We have carefully compared our results with those of the Alpha Collaboration and are not able to fully resolve the discrepancies. However, there are a number of issues in the respective analyses which serve to reduce the differences between our respective results.

We first observe that the Alpha analysis for $\alpha_5$ makes use of a linear fit to the ratio $R_F(x)$ where

$$R_F(x)=f_A(m_q)/f_A(m_{q\text{ref}}), \quad x=m_q/m_{q\text{ref}}. \tag{46}$$

A large reference mass of order $m_q=m_s$ is chosen to avoid anomalous infrared sensitivity in the quenched theory. However, their analysis of the slope of $R_F(x)$ neglects a factor of

$$\frac{1}{1+y_{\text{ref}}\,\frac{1}{2}\,\alpha_5} \tag{47}$$

[cf. Eqs. (3.7)–(3.9) of [8]] reflecting the difference between $\chi$PT as an expansion about the massless limit and their use of a large reference mass. Including this factor would increase their estimate of $\alpha_5$ by about 20%,

$$\alpha_5(\text{corrected})=1.18(7). \tag{48}$$

If only statistical errors are considered, this estimate is still significantly below our values for $\alpha_5$.

The Alpha ratio method is insensitive to mass independent renormalization factors such as $Z_A$ but requires knowledge of the physical scale and inputs the physical value of $f_\pi=93.3$ MeV. In the case that $f_A$ is well described by a linear function (as is seen in the Alpha analysis), the Alpha ratio method and our second method (using the ratio of the slope and intercept) should give compatible results. However, we do use somewhat different values for the physical scale parameters, etc.

To make a more precise connection with the Alpha analysis we can present our results using scale and renormalization factors determined from interpolating formulas fitted by the Alpha Collaboration. Although determined from data on finer lattice spacing than our lattices, the nonperturbative interpolating formulas for the scale factor, $1/a$, and the renormalization constant, $Z_A$, are relatively smooth and yield the extrapolated values

$$1/a = 1.184 \text{ GeV}, \quad Z_A = 0.7594, \quad \beta = 5.7 \tag{49}$$

and

$$1/a = 1.811 \text{ GeV}, \quad Z_A = 0.7827, \quad \beta = 5.9. \tag{50}$$

Using these values of the scale and renormalization constants our fits for $f_A$ [in Eqs. (38), (39)] become (in GeV units)

$$f_A = \sqrt{2}[0.0938(10) + 0.059(3)m_\pi^2], \quad \beta = 5.7 \tag{51}$$

and

$$f_A = \sqrt{2}[0.0926(12) + 0.053(4)m_\pi^2], \quad \beta = 5.9. \tag{52}$$

With these normalization factors we see that the physical value of $f_\pi$ is well reproduced which implies that our two methods for determining $L_5$ ($\alpha_5$) are in agreement yielding

$$L_5(10^3) = 1.39(6), \quad \alpha_5 = 1.75(8), \quad \beta = 5.7 \tag{53}$$

and

$$L_5(10^3) = 1.24(8), \quad \alpha_5 = 1.57(11), \quad \beta = 5.9. \tag{54}$$

The values of $\alpha_5$ are somewhat below our previous values but are still above the continuum values given by the Alpha Collaboration. The remaining systematic difference between our calculation and the Alpha analysis concerns the clover coefficients, $C_{sw}$, used to make the $O(a)$ improvement. The nonperturbative Alpha analysis of the clover coefficient yields an interpolating formula which becomes rather unstable when extrapolated to our coarse lattices. The Fermilab analysis uses values of the clover coefficient of $C_{sw} = 1.57$ and 1.50 for $\beta = 5.7$ and 5.9, respectively. These values are considerably less than those suggested by the Alpha analysis and could imply a sizable $O(a)$ dependence in the parameters of our effective action and affect our comparisons with the Alpha Collaboration continuum result. We are not able to address this question further in the present analysis. Note that the focus of our analysis has been to determine appropriate effective actions that describe the infrared physics of lattice field theories on fixed lattices and we do not address the question of the continuum limit of such theories.

Finally we note that caution is required in any direct comparison between the quenched and unquenched values of $\alpha_5$. We have emphasized that there are no quenched chiral logs which affect the extrapolation of $f_A(m_\pi^2)$ for equal quark masses. However there is a strong chiral log effect in the unquenched theory. The Gasser and Leutwyler analysis [14] of the one-loop chiral logs determines $L_5$ ($\alpha_5$) from the physical value of $f_K/f_\pi$,

$$\alpha_5 = 2.8 \pm 0.6 - 3\ln(\mu/m_\eta). \tag{55}$$

Hence, $\alpha_5 = 0.5$ for a large normalization scale, $\mu = 4\pi f_\pi$, $\alpha_5 = 0.99$ for $\mu = 1$ GeV and $\alpha_5 = 1.76$ for $\mu = m_\rho$. The continuum limit of the quenched theory corresponds to the leading order of the $1/N_c$ expansion of the full theory which cannot be isolated phenomenologically from the higher order contributions.

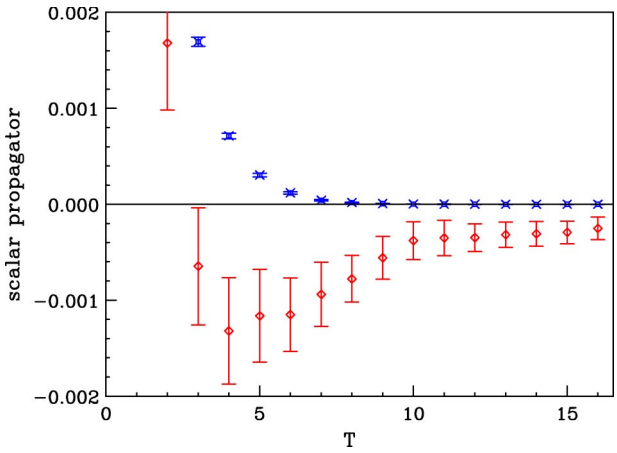


FIG. 9. Isovector scalar correlator for the $\beta = 5.9$ $16^3 \times 32$ lattices. The lightest ($\kappa_q = \kappa_{\bar{q}} = .1397$)($\diamond$) and heaviest ($\kappa_q = \kappa_{\bar{q}} = .1382$)($\times$) correlators are shown.

## VI. THE QUENCHED SCALAR PROPAGATOR

One of the most dramatic effects of quenched chiral loops is observed in the scalar valence propagator. The behavior of this propagator for the $\beta = 5.7$ ensemble was studied in [5]. There it was found that the propagator was well described as a combination of a short-range positive exponential associated with a heavy ($>1$ GeV) scalar $\bar{q}q$ meson state and a long-range *negative* tail arising from the $\eta'$-$\pi$ intermediate state. In the quenched approximation, the $\eta'$-$\pi$ loop diagram exhibits not just a quenched chiral logarithm, but a quenched chiral *power*, with infrared behavior $\sim d^4p/p^6$. This long-range component is well described in both shape and magnitude by the finite-volume $\eta'$-$\pi$ loop calculation. [Note: In the $\beta = 5.7$ results, the $\approx 2$ standard deviation discrepancy between the data and the $\chi$PT calculation for $t > 7$ (cf. Fig. 10 of Ref. [5]) we now believe to be a statistical fluctuation. See below.] As discussed in [5] the one-loop term that dominates the scalar propagator at small quark mass is determined with no adjustable parameters by the chiral Lagrangian parameters $m_\pi, f$, and $r_0$, already fixed from the analysis of the pseudoscalar sector. In particular, the long-range scalar propagator exhibits a very strong mass dependence in the light quark regime, which is very well explained by the dependence of the finite volume one loop contribution on pion mass squared.

The analysis of the scalar correlator for $\beta = 5.9$ confirms the main conclusions of Ref. [5] (see Figs. 9 and 10). For the 5.9 ensemble, we find excellent agreement between the long-range behavior of the correlator and the Q$\chi$PT loop calculation (which contains no adjustable parameters), with the theoretical formula matching the data all the way out to the largest time separation of $t = 16$. The details of the analysis of the $\beta = 5.7$ data were discussed in [5]. The $\beta = 5.9$ ensemble was analyzed similarly, though with some simplifications. First, in [5] both smeared and local sources were used, and a factorization procedure allowed an estimate of the

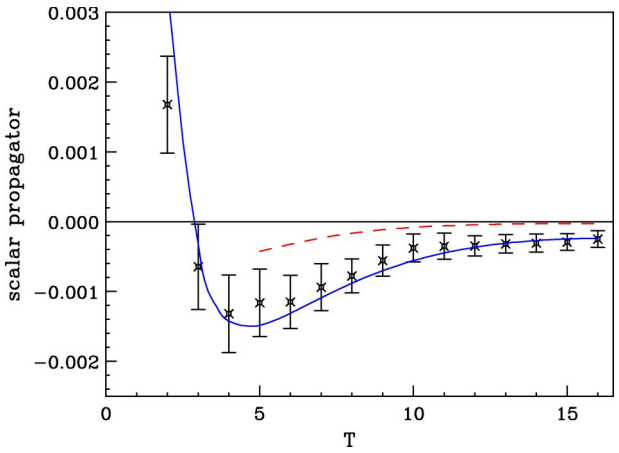


FIG. 10. The scalar correlator for $\beta=5.9$ and $\kappa=.1397$. The solid line is a fit consisting of the sum of a scalar meson pole and an $\eta'$-$\pi$ loop diagram. The dashed line is the loop term in the infinite volume limit.

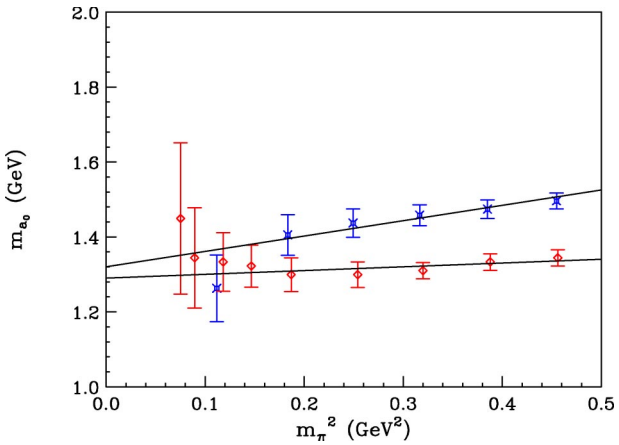


FIG. 11. Mass of the $a_0$ meson for $\beta=5.7$ (boxes) and $\beta=5.9$ ($\times$'s).

mass of the excited $a_0^*$ meson. This produced a good fit to the scalar correlator all the way down to $t=1$. For the analysis of the 5.9 data, we have not carried out an independent estimate of the excited $a_0^*$ contribution, but have simply rescaled the parameters obtained from the 5.7 analysis, holding this contribution fixed in the fits which determine the ground state $a_0$ parameters. For the 5.9 data we used a time range $t\geqslant 3$, so the fits were insensitive to the choice of excited state parameters. The other difference in the 5.9 analysis is that the lightest pion mass (330 MeV) is somewhat heavier than that for the 5.7 study (275 MeV). In [5] the formula used to parametrize the $\eta'$-$\pi$ contribution was obtained by resumming iterated bubble graphs to all orders. In the analysis of the 5.9 data, we have found that only the one-loop graph is significant, so we have discarded higher order bubbles in the formula used to fit the correlator. Thus, defining the time-dependent zero-momentum scalar correlator as

$$\Delta(t)\equiv\sum_{\vec{x}}\langle\overline{\psi}_1\psi_2(\vec{x},t)\overline{\psi}_2\psi_1(0)\rangle \tag{56}$$

we fitted the lattice correlator to the function [cf. Eq. (14) of Ref. [5]]

$$\Delta(t)\sim 32r_0^2\frac{f_s^2}{2m_s}e^{-m_s t}+4r_0^2\tilde{B}_{hp}(t) \tag{57}$$

where $\tilde{B}_{hp}(t)$ is the $\vec{p}=0$ Fourier transform of the $\eta'$-$\pi$ bubble graph, calculated in a finite volume:

$$B_{hp}(p)=\frac{1}{VT}\sum_k\frac{1}{[(k+p)^2+m_\pi^2]}\frac{-m_0^2}{(k^2+m_\pi^2)^2}. \tag{58}$$

Note that $m_\pi$, $r_0$, and $m_0$ are already determined from the pseudoscalar correlator analysis, so the only two fit parameters are the scalar mass and decay constant $m_s$ and $f_s$. In Fig. 10 we show the data for the scalar correlator at $\beta=5.9$ and the lightest quark mass, $\kappa=.1397$, along with a fit given by the function (57).

The mass of the $a_0$ meson obtained from our fits is plotted in Fig. 11. In the chiral limit we obtain (using the rho scale)

$$m_{a_0}=1285(60)\ \text{MeV at}\ \beta=5.7 \tag{59}$$

$$=1326(86)\ \text{MeV at}\ \beta=5.9. \tag{60}$$

In the chiral loop calculation of the $\eta'$-$\pi$ intermediate state contribution, we have included the effect of finite physical volume, replacing momentum integrals by discrete sums. For the lightest pion masses the finite volume effect is quite large, due to the singular infrared behavior of the loop contribution. It is interesting to note that the Monte Carlo results for the scalar correlator agree quite nicely with the prediction of *finite volume* Q$\chi$PT, but disagree significantly with the corresponding infinite volume calculation. This strong finite volume effect is also seen by the RBC Collaboration [20]. The dashed line in Fig. 10 is the infinite volume loop calculation. For $t>5$, the correlator is dominated by the $\eta'$-$\pi$ loop, and it is clear that the Monte Carlo result exhibits the predicted enhancement from the finite volume effect. From the point of view of Dirac eigenmodes, the finite volume dependence predicted by $\chi$PT arises from a subtle interplay between exact zero modes and near zero modes. In the infinite volume limit, the contribution of exactly zero modes vanishes, but for finite volume these modes are essential for reproducing the correct chiral behavior. Since the MQA pole shifting ansatz consists of repositioning some exactly zero modes, it is reassuring to see that the resulting correlators exhibit excellent agreement with the finite volume effect predicted by Q$\chi$PT.

Finally, the scalar decay constant, $f_s$, of the $a_0$ meson obtained from our fits is plotted in Fig. 12. In the chiral limit we obtain (using the rho scale)

$$f_s=64(5)\ \text{MeV at}\ \beta=5.7 \tag{61}$$

$$=68(3)\ \text{MeV at}\ \beta=5.9. \tag{62}$$

## VII. CONCLUSIONS

The lattice calculations described in this paper and our previous work [4–6] have focused on the chiral properties of

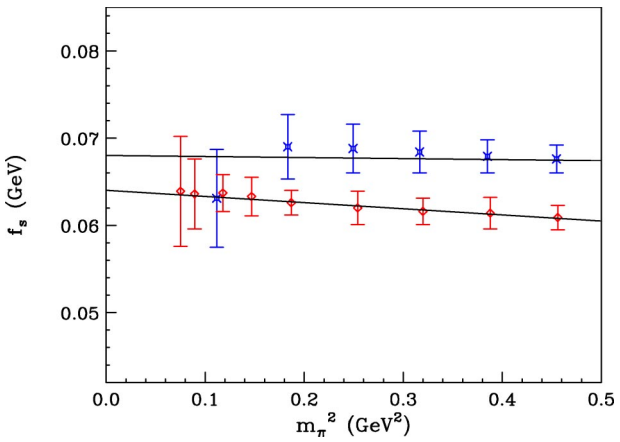


FIG. 12. The scalar decay constant of the $a_0$ meson for $\beta=5.7$ (boxes) and $\beta=5.9$ ($\times$'s).

meson correlators in the flavor singlet and nonsinglet pseudoscalar and nonsinglet scalar channels. In addition to exhibiting for the first time a number of anomalous chiral effects due to quenching, the results have confirmed a level of overall consistency of the low energy chiral Lagrangian description of meson properties in QCD, and provided quantitative estimates of the relevant chiral Lagrangian parameters.

A central feature of this study is the accurate calculation of the pseudoscalar flavor-singlet hairpin insertion responsible for the gluonic component of the $\eta'$ mass. In this calculation the MQA pole shifting ansatz has a particularly salutary effect. Since the pseudoscalar hairpin insertion arises from the $U_A(1)$ anomaly, it is particularly sensitive to topological features of the gauge field. As a result, the exceptional configuration problem in the hairpin is even more serious than in the valence correlators. The MQA procedure allows the first detailed study of the time dependence of the hairpin correlator. The most striking feature of this time dependence is that it is quite accurately described *at all time separations* by a the simple chiral Lagrangian diagram consisting of two pion propagators on either side of a momentum independent mass insertion. Values obtained for the field renormalization parameter $\alpha_\Phi$, which parametrizes the momentum dependence of the hairpin insertion, are very small and consistent with zero. Perhaps even more remarkable is the fact that the hairpin correlator exhibits an absence of excited state contamination, with the ground-state double-pole diagram giving a complete description of the correlator. This result is confirmed not only by the time dependence of the hairpin correlator, but also by a detailed comparison of hairpin and valence correlators with both smeared and local sources, as discussed in Ref. [4]. Since we know from the valence correlator that the local $\bar{\psi}\gamma^5\psi$ operator creates a state which includes a substantial excited state component along with the ground state pion, we conclude that these excited states are decoupled from the hairpin vertex itself. This may be viewed as a plausible extension of the OZI rule [21]. Calculation of vector and axial-vector hairpin correlators [22] has confirmed that $q\bar{q}$ annihilation in these channels is highly suppressed compared to the anomaly-enhanced pseudoscalar hairpin diagram, as expected from OZI phenomenology. The absence of evidence for excited states in the pseudoscalar hairpin indicates that annihilation from these excited pseudoscalar states is similarly OZI suppressed. Only if the $q\bar{q}$ are in a Goldstone state do they have an unsuppressed pair-annihilation amplitude. The possibilities for extending these calculations to investigate the details of the connection between quark pair creation and annihilation and topological charge fluctuations are intriguing.

A global fit to the pseudoscalar masses and decay constants obtained from the valence (nonsinglet) correlators as a function of the quark masses yields an estimate of the quenched chiral log parameter $\delta$, the pion decay constant $f_\pi$, the slope parameter $r_0$, and the Leutwyler parameters $L_5$ and $L_8$ (Table III). We have found that a chiral Lagrangian analysis at the one-loop level provides a good description of the data over the range of masses studied, for both equal and unequal quark masses. The fit values of the quenched chiral log parameter $\delta$, $\sim$.05–.06, are rather small, but consistent with the values obtained directly from the hairpin diagram, averaged over the mass region studied. The chirally extrapolated value of $\delta$ ($\sim$.10) evaluated from the hairpin correlator is somewhat larger, but still smaller than the phenomenological estimate of $\sim$0.17. There may be some indication (cf. Fig. 2) that the value of $\delta$ is increasing for smaller lattice spacing so that, in the continuum limit, it might be closer to the phenomenological estimate. Similarly, the values of $L_5$ ($\alpha_5$) we obtain are somewhat larger than the recent results of Heitger *et al.* [8]. In any case, since the lattice spacings we have studied are fairly coarse, the overall consistency of our fits suggests that, even for finite lattice spacing, the low energy dynamics is well described by a chiral Lagrangian, with the main lattice spacing effects consisting of corrections to the Lagrangian parameters.

The behavior of the nonsinglet scalar propagator at light quark mass provides a particularly dramatic probe of chiral dynamics, and the success of the chiral Lagrangian description (Sec. VI) is impressive. The prominent $\eta'$-$\pi$ loop contribution is completely determined in terms of the chiral parameters $m_\pi$, $r_0$, and $m_0$, extracted from the pseudoscalar analysis. The loop calculation agrees well with the lattice data in magnitude, time dependence, and pion mass dependence. For the box size ($\sim$2 fm) and pion masses we have used, the loop diagram exhibits a strong finite volume effect, and the agreement with the data is satisfactory only if the loop calculation is carried out in a finite volume. It would be interesting to carry out the numerical scalar propagator calculation on different size lattices to explicitly observe this finite volume effect. In view of the agreement we see on a single size box over a wide range of pion masses, we would expect the chiral loop diagram to also give a good description of the finite volume dependence, as long as the box is still large compared to the QCD scale. The sensitivity of the $\eta'$-$\pi$ loop diagram to finite volume effects makes it especially useful for probing the role of zero modes in finite volume calculations. For extremely large boxes (large compared to the chiral scale), zero modes and global topology should be irrelevant, e.g. ensemble averages over any fixed topology should converge to the same result in the infinite volume limit. On the other hand, for volumes which are large

with respect to the QCD scale but still comparable to the chiral scale, the exact zero modes contribute in an essential way to the dynamics described by the chiral Lagrangian. The techniques developed here can easily be used to study the role of zero modes and global topology in finite volume chiral dynamics. This can be done, for example, by studying the contributions to the ensemble average for various correlators as a function of the global topological charge. We have seen that the integrated anomaly method of Smit and Vink [17], after MQA improvement, provides a convenient way of estimating the global topological index $\nu$ of a configuration. Calculation of $\nu$ using exactly chiral (e.g. overlap or domain wall) fermions would be ideal, but the approach used here based on clover improved Wilson fermions is more economical and appears to be quite effective for studying issues which do not depend crucially on having exactly integer valued $\nu$'s. For example, the results for the topological susceptibility (Sec. IV) are in good agreement with other estimates. It would be interesting to carry out a more detailed investigation of the scalar and pseudoscalar correlators studied here, decomposing the ensemble averages into various topological charge sectors. This would provide useful insight into the role of global topology in chiral dynamics at finite volume.

After properly accounting for quenched chiral effects in the scalar propagator, the $a_0$ masses (at $\kappa_c$) are extracted. The results, $m_{a_0}=1.33(5)$ and 1.29(6) GeV for $\beta=5.9$ and 5.7, respectively are considerably larger than the observed $a_0(980)$ resonance mass. The value for $m_{a0}=1.33(5)$ GeV suggests that there is a large effect when internal quark loops are included or that the observed $a_0(980)$ resonance is a distinct state, possibly a $K\overline{K}$ "molecule" (which would not appear in the quenched approximation), and not an ordinary $q\overline{q}$ meson.

## ACKNOWLEDGMENTS

The work of W.B. and E.E. was performed at the Fermi National Accelerator Laboratory, which is operated by University Research Association, Inc., under contract DE-AC02-76CHO3000. The work of H.T. was supported in part by the Department of Energy under grant DE-FG02-97ER41027.

[1] S.R. Sharpe and N. Shoresh, Phys. Rev. D **62**, 094503 (2000).
[2] C. Bernard and M. Golterman, Phys. Rev. D **46**, 853 (1992).
[3] S. Sharpe, Phys. Rev. D **46**, 3146 (1992); **46**, 853 (1992).
[4] W. Bardeen, A. Duncan, E. Eichten, and H. Thacker, Phys. Rev. D **62**, 114505 (2000).
[5] W. Bardeen, A. Duncan, E. Eichten, N. Isgur, and H. Thacker, Phys. Rev. D **65**, 014509 (2002).
[6] W. Bardeen, E. Eichten, and H. Thacker, Nucl. Phys. B (Proc. Suppl.) **119**, 242 (2003).
[7] H. Wittig, Nucl. Phys. B (Proc. Suppl.) **119**, 242 (2003).
[8] ALPHA Collaboration, J. Heitger, R. Sommer, and H. Wittig, Nucl. Phys. **B588**, 377 (2000).
[9] W. Bardeen, A. Duncan, E. Eichten, G. Hockney, and H. Thacker, Phys. Rev. D **57**, 1633 (1998).
[10] ALPHA Collaboration, R. Frezzotti, S. Sint, and P. Weisz, J. High Energy Phys. **07**, 048 (2001); Alpha Collaboration, R. Frezzotti, P.A. Grassi, S. Sint, and P. Weisz, *ibid.* **08**, 058 (2001).
[11] R. Narayanan and H. Neuberger, Phys. Rev. Lett. **71**, 3251 (1993); Nucl. Phys. **B443**, 305 (1995).
[12] D.B. Kaplan, Phys. Lett. B **288**, 342 (1992).
[13] CP-PACS Collaboration, V.I. Lesk *et al.*, Nucl. Phys. B (Proc. Suppl.) **119**, 691 (2003).
[14] J. Gasser and H. Leutwyler, Nucl. Phys. **B250**, 465 (1985).
[15] S.J. Dong, T. Draper, I. Horvath, F.X. Lee, K.F. Liu, N. Mathur, and J.B. Zhang, hep-lat/0304005.
[16] Y. Kuramashi, M. Fukugita, H. Mino, M. Okawa, and A. Ukawa, Phys. Rev. Lett. **72**, 3448 (1994).
[17] J. Smit and J.C. Vink, Nucl. Phys. **B286**, 485 (1987).
[18] G.P. Lepage and P.B. Mackenzie, Phys. Rev. D **48**, 2250 (1993).
[19] T. Bhattacharya and R. Gupta, Phys. Rev. D **54**, 1155 (1996); A.X. El-Khadra, A.S. Kronfeld, P.B. Mackenzie, S.M. Ryan, and J.N. Simone, *ibid.* **58**, 014506 (1998).
[20] RBC Collaboration, S. Prelovsek and K. Orginos, Nucl. Phys. B (Proc. Suppl.) **119**, 822 (2003).
[21] G. Zweig, CERN Report No. 8419 TH 412, 1964, reprinted in *Developments in the Quark Theory of Hadrons*, edited by D.B. Lichtenberg and S.P. Rosen (Hadronic Press, Massachusetts, 1980); S. Okubo, Phys. Lett. **5**, 165 (1963); Phys. Rev. D **16**, 2336 (1977); J. Iizuka, K. Okada, and O. Shito, Prog. Theor. Phys. **35**, 1061 (1966); J. Iizuka, Suppl. Prog. Theor. Phys. **37–38**, 21 (1966).
[22] N. Isgur and H.B. Thacker, Phys. Rev. D **64**, 094507 (2001).